Periodica Polytechnica Electrical Engineering and Computer Science, 65(4), pp. 394–403, 2021

Optimum Switching Angles Control of SRM for Electric Vehicle Applications

Laith Al Quraan[1*], Laszlo Szamel[1], Mahmoud Hamouda[1,2]

[1] Department of Electric Power Engineering, Faculty of Electrical Engineering and Informatics, Budapest University of Technology and Economics, H-1111 Budapest, Egry József utca 18., Hungary
[2] Electrical Engineering Department, Faculty of Engineering, Mansoura University, 35516 Mansoura, El Gomhouria street 25, Egypt
* Corresponding author, e-mail: alquraan.laith@vet.bme.hu

Received: 05 December 2020, Accepted: 18 February 2021, Published online: 12 October 2021

Abstract

Switched Reluctance Motor (SRM) drive is being gradually used in industrial applications, including electric vehicles (EVs), due to several advantages over conventional motors. However, the nonlinear magnetic characteristics of the motor make its controller very complicated. This paper presents a simplified procedure to obtain the optimal switching angles under hysteresis current control SRM drive over a wide range of speeds. A multi-objective optimization technique is applied to determine the optimal switch on and switch off angles that achieve the optimum combination of maximum average torque with minimum torque ripple and copper loss. A searching algorithm is developed for each operating point to define the maximum average torque and the minimum torque ripple and copper losses, as they vary for different currents and motor speeds. Then the optimal values of switching angles are stored in the lookup tables to build a MATLAB model of the SRM drive system. Finally, simulation and experimental results are presented to show the validity and effectiveness of the proposed controller.

Keywords

optimization, Switch Reluctance Motor, electric vehicles, switching angles

1 Introduction

The Switched Reluctance Motor (SRM) represents a promising candidate for electric vehicle (EV) application due to its simple and robust structure, low manufacturing cost, high fault-tolerant ability, and wide speed range of operation [1–4]. Despite these features, the main blocking factors of widespread SRM drive are the significant torque ripple, vibration, and acoustic noise comparable to the conventional machines [5–7]. The reduction of torque ripple can be realized by improving the motor's mechanical design and using advanced control techniques [7].

The analysis and control of the SRM is a complicated task because of the doubly salient structure and highly nonlinear magnetic characteristics of the motor [8, 9]. For EV applications, the maximum torque production is required over a wide range of speed to overcome the starting friction and provide the climbing capability [10]. Furthermore, drive efficiency should be improved to extend the car range, and the torque ripple should be reduced to prevent speed fluctuations [11]. However, obtaining the best values of all quantities simultaneously, such as average torque and torque ripple, in the SRM drive is impossible. Still, the proper selection of switch-on (θ_{on}) and switch-off (θ_{off}) angles along with the current controller can improve the torque production and energy efficiency of the SRM drive.

Many studies have been conducted on the optimum selection of switching angles (θ_{on} and θ_{off}) of SRM drive according to several goals, such as improving the torque production, torque ripple, and electric efficiency. In [5], the control parameters were optimized in order to reduce the torque ripple and the speed error of the SRM drive. In [12], an automatic switch-on angle controller is designed by making the phase current reaches its peak at the beginning overlapping angle between the rotor and stator poles to increase the torque/current ratio. Analytical approaches have been presented in [13–15] to calculate the optimal switching angles that improve the SRM efficiencies over a wide range of speed. In [16], a switching angles controller for the low-speed operation of SRM has been presented based on offline optimization of switch-off angle to minimize the torque ripple and copper losses. In contrast,

Cite this article as: Al Quraan, L., Szamel, L., Hamouda, M. "Optimum Switching Angles Control of SRM for Electric Vehicle Applications", Periodica Polytechnica Electrical Engineering and Computer Science, 65(4), pp. 394–403, 2021. https://doi.org/10.3311/PPee.17640

the switch-on angle is regulated online according to the sequential phase currents' crossing approach. In [17], the average torque control method has been developed by the online determination of excitation angles to achieve current-controlled SRM drives' optimum performance in terms of torque ripple and motor efficiency. In [18], different optimization procedures are proposed to optimize the conduction angle in the SRM drive for improving the output torque, torque ripple, and motor efficiency. In [19], the direct instantaneous torque control (DITC) with a different selection of switch-off angle is proposed to improve torque ripple and speed response in SRM drive. The switching angles were optimized to enhance the torque ripple and electric efficiency of the SRM drive in [20]. The control parameters of varying angles control were optimized to suppress the SRM noise in [21]. The performance optimization for a wide range of SRM drive speed under the single pulse controller is investigated in [22] through online adjustment of switching angles. In [23], a genetic optimization algorithm that utilizes the electromagnetic vibration data is used to obtain the optimum switching angles to minimize the torque ripple in SRM drive.

In this paper, a multi-objective optimization technique is implemented to realize the optimum switching angles (θ_{on} and θ_{off}) of SRM drive, aiming to achieve the maximum average torque with minimum torque ripple and copper losses over a wide speed range. A searching algorithm is developed for each operating point to define the base values of torque ripple, average torque, and copper loss as they vary for different current and motor speed. After that, the optimum values of switching angles are utilized to build lockup tables in order to evaluate the motor performance at different operating conditions.

The mathematical modeling and fundamental equations of SRM are presented in Section 2 of this paper. The analytical method for determining the optimal switching angles is given in Section 3. The optimization technique and the proposed controller are described in Sections 4 and 5. Section 6 presents the simulation results and the verification of experiments. Finally, in Section 7, the conclusions drawn from this research are discussed.

2 Modeling and magnetic characteristic of SRM

Accurate determination of the magnetic characteristics is critical for modeling and control the SRM. However, the SRM has nonlinear magnetic attributes because of its doubly salient construction and highly saturated magnetic circuit [24, 25]. Such characteristics are mostly determined using analytical methods, Finite Element Method (FEM), and experimental measurements [26–28]. The analytical methods are very complicated and often involve simplifications assumptions, which significantly impact its accuracy [26]. The FEM is widely accepted to calculate the magnetic characteristics of the SRM. Still, this method needs precise geometrical data and material properties of the SRM, which are not provided by the manufacturer in most scenarios [26–29]. On the other hand, the experimental measurements correspond to the actual machine data and provide the highest accuracy among these methods.

In this study, the indirect measurement is used to calculate the developed torque $T(i,\theta)$, phase inductance $L(i,\theta)$, and flux linkage $\lambda(i,\theta)$.These data are stored in the form of lookup tables to build an accurate MATLAB simulation model. Full details about the measuring process are discussed in [27]. The inspected machine is four phases 8/6 SRM, whose data are given in Table 1. The measured magnetic characteristics of the tested SRM are shown in Fig. 1. The fully aligned position in mechanical degree is defined at $\theta=0°$, while $\theta=30°$ represents the unaligned position.

The phase voltage of SRM can be calculated as follow:

$$V = R \cdot i + L(i,\theta) \cdot \frac{di}{dt} + e, \tag{1}$$

$$e = \frac{dL(i,\theta)}{d\theta} \cdot i \cdot \omega, \tag{2}$$

where V, R, i, L, ω, and θ represent the phase voltage, stator resistance, phase current, back EMF, inductance, rotor speed (rad/sec), and rotor position, respectively.

The phase torque (T_{ph}) of SRM is given by:

$$T_{ph} = \frac{1}{2} i^2 \cdot \frac{dL(i,\theta)}{d\theta}. \tag{3}$$

The total torque (T_e) of SRM is the summation of phase's torques:

$$T_e = \sum_m T_{ph}. \tag{4}$$

Table 1 Four phases 8/6 SRM data

Rated voltage	600 V
Output power	4 kW
Rated speed	1500 rpm
Unaligned inductance (L_u)	13.5 mH
Winding resistance	0.642 Ω
θ_m	7.5°
θ_z	30°
Air gap length	0.4 mm
Turns per pole	88

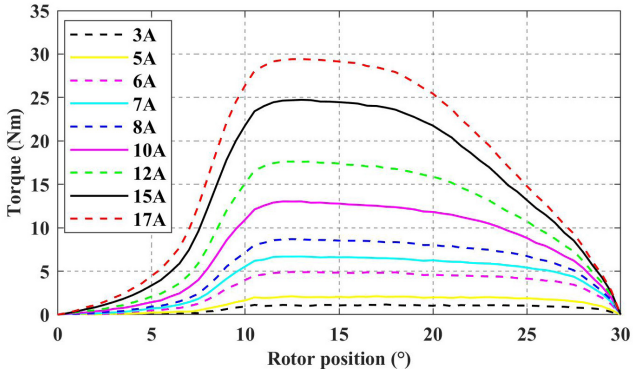

(a)

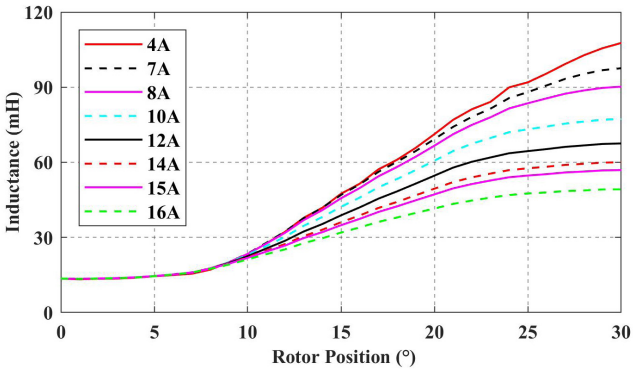

(b)

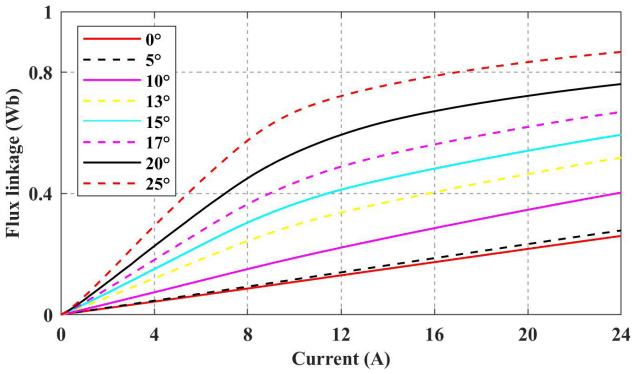

(c)

Fig. 1 The measured magnetic characteristics; (a) Torque $T(i,\theta)$; (b) Inductance $L(i,\theta)$; (c) Flux $\lambda(i,\theta)$.

The average torque is derived by integrated the total torque over one electric cycle as follows:

$$T_{avg} = \frac{1}{\tau}\int_0^{\tau} T_e(t)\cdot dt, \tag{5}$$

with,

$$\tau = \frac{60}{n\cdot N_r}, \tag{6}$$

where, τ is the fundamental period time of one electric cycle, N_r is the number of rotor poles, and n is the rotor speed in rpm.

The torque ripple (T_{rp}) is determined by dividing the difference between maximum and minimum of total torque by average torque:

$$T_{rp} = \frac{T_e(\max) - T_e(\min)}{T_{avg}}. \tag{7}$$

The copper losses (P_{cu}) in stator windings are determined as:

$$P_{cu} = m\cdot I^2 R, \tag{8}$$

and,

$$I = \sqrt{\frac{1}{\tau}\int_0^{\tau} i_{ph}^2(t)\cdot dt}, \tag{9}$$

where m, and i_{ph} are I the number of phases, the phase current and the RMS phase current, respectively.

3 Problem description

Referring to Eq. (3), the torque produced by each phase depends on the inductance slop and current magnitude. As shown in Fig. 2, a linear inductance profile is used to simplify the analysis of torque production in SRM. The inductance profile can be divided into three periods according to the inductance slope:

1. Constant period $(dL/d\theta \cong 0)$: the electromagnetic torque is almost zero.

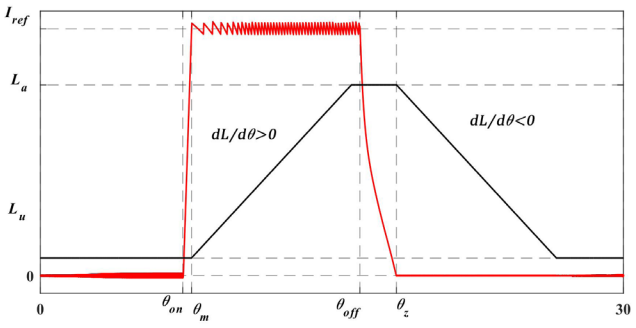

(a)

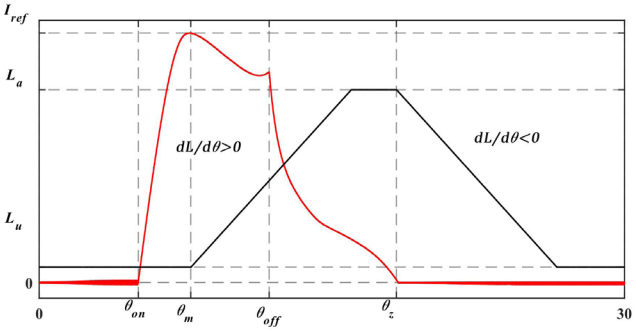

(b)

Fig. 2 Current waveform and linear inductance waveform; (a) At low speed operation; (b) At high speed operation.

2. Increasing period $(dL/d\theta > 0)$: the positive torque (motoring) is produced by exited the motor's coils in this zone.
3. Decreasing period $(dL/d\theta < 0)$: the negative torque (braking) is produced by exited the motor's coils in this zone.

Hence, to ensure maximum efficiency, the phase current must reach its peak at θ_m, where the rotor pole begins to overlap with the rotor pole, and return to zero at θ_z to avoid producing negative torque [13–15]. Therefore, the switching angles (θ_{on} and θ_{off}) should be adjusted according to the reference current and motor speed to satisfy the conditions mentioned above.

3.1 Determination of switch on angle

The switch-on angle based on the assumption of constant inductance in minimum inductance region can be calculated as following [13–15, 28]:

$$\theta_{on} = \theta_m - \frac{L_u \cdot I_{ref} \cdot \omega}{V_{dc}}, \tag{10}$$

where L_u, V_{dc}, ω and I_{ref} are the minimum inductance, the supply voltage, the motor speed, and the reference current, respectively.

Equation (10) neglects the back EMF effect during the minimum inductance region, but the back EMF raises as the motor speed increase.

As a result, the back EMF prevents the phase current from reaching its peak value at θ_m, and the equation starts to break down.

Accurate determination of the switch-on angle with represent of the effect of back EMF is given in [15] as follow.

By solving Eq. (1) for the phase current, yields:

$$i(t) = \frac{V_{dc}}{R + (dL/d\theta)\omega} + \left[I_o - \frac{V_{dc}}{R + \omega(dL/d\theta)} \right] e^{-t/\tau}, \tag{11}$$

and,

$$\tau = \frac{L(\theta)}{R + \omega(dL/d\theta)}. \tag{12}$$

Then the current rise time (t) can be calculated as:

$$t = \frac{\theta_m - \theta_{on}}{\omega}. \tag{13}$$

By substituting Eq. (13) into Eq. (11):

$$\frac{i}{V_{dc}}\left(R + (dL/d\theta)\omega\right) = 1 - e^{-t/\tau}. \tag{14}$$

So the formula of (θ_{on}) that realize the first peak of phase current at θ_m can be written as:

$$\theta_{on} = \theta_m + \frac{L(\theta)}{R + \omega(dL/d\theta)} \ln\left[1 - \frac{i}{V_{dc}}\left(R + \omega(dL/d\theta)\right) \right]. \tag{15}$$

Equation (15) gives the θ_{on} over the entire range speed with the consideration of back EMF. Optimal θ_{on} can be achieved by accurate determination of L_u and its derivative which can be obtained accurately by the curve fitting method.

3.2 Determination of switch off angle

A simple calculation procedure for the θ_{off} under the single pulse controller can be implemented according to the assumption that the rising and falling times of flux are equal, as shown in Fig. 3 [13–15].

The flux-linkage rising time (t_{rise}) and the flux-linkage falling time (t_{fall}) are given as:

$$t_{rise} = \frac{\theta_{off} - \theta_{on}}{\omega} = t_{fall} = \frac{\theta_z - \theta_{off}}{\omega}. \tag{16}$$

From Eq. (16), the can be written as:

$$\theta_{off} = \frac{\theta_{on} + \theta_z}{2}. \tag{17}$$

Equation (17) is derived at high-speed operation under a single pulse controller. However, Eq. (17) starts affected by the current chopping mode at low speed operation, leading to increased error as the motor speed decreases. This error can be handled by adding a compensation term as following [15]:

$$\theta_{off} = \frac{\theta_{on} + \theta_z}{2} + \frac{k}{\omega I_{ref}}, \tag{18}$$

where, k is a constant that can be fitted with reference current and motor speed. However, the analytical methods presented in Section 3 are not suitable for EV applications

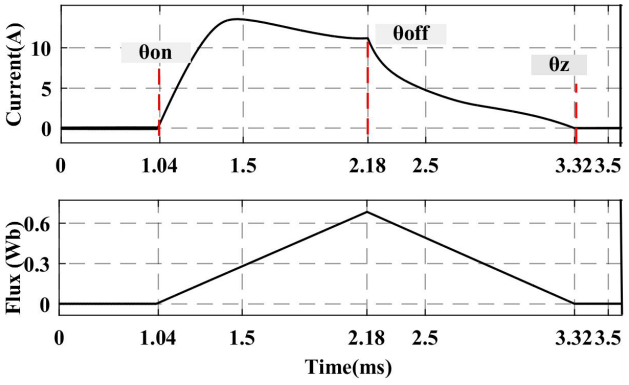

Fig. 3 Current and flux waveforms at high speed.

due to the simplified hypothesis, which leads to inaccurate solutions. Furthermore, it does not take the average torque and the effect of torque ripple on the account.

4 The optimization problem

This study aims to find the appropriate switching angles that provide the maximum average torque with minimum torque ripple and copper losses. Even so, realizing all these goals simultaneously is impossible because each goal needs different switching angles. For the sake of realizing the optimum combination of maximum average torque with minimum torque ripple and copper loss, a multi-objective optimization function involving three objectives is employed as follow:

$$F_{obj}\left(\theta_{\text{on}},\theta_{\text{off}}\right)=\min\left(w_T\frac{T_b}{T_{avg}}+w_r\frac{T_r}{T_{rb}}+w_{cu}\frac{P_{cu}}{P_{cub}}\right), \tag{19}$$

$$w_T+w_{rb}+w_{cub}=1, \tag{20}$$

where F_{obj} denotes the multi-objective optimization function. T_b and w_T are the base value and weight factor of average torque. T_{rb} and w_{rb} are the base value and weight factor of torque ripple. P_{cub} and w_{cub} are the base value and weight factor of copper losses.

The base values for related criterion at a specific operating point are determined as follow:

$$P_{cub}\left(\theta_{\text{on}},\theta_{\text{off}}\right)|\,\omega,I_{ref}=\min\left(P_{cu}\right), \tag{21}$$

$$T_{rb}\left(\theta_{\text{on}},\theta_{\text{off}}\right)|\,\omega,I_{ref}=\min\left(T_r\right), \tag{22}$$

$$T_b\left(\theta_{\text{on}},\theta_{\text{off}}\right)|\,\omega,I_{ref}=\max\left(T\right). \tag{23}$$

In order to determine the base values for all operating points, a searching algorithm is applied by changing the switching angles step by step for each operating point, as shown in Fig. 4. The average torque, torque ripple, and copper losses are calculated and saved for every stage by the simulation model. After that, the average torque's base value is defined as the highest average torque, while the lowest values of the torque ripple and copper losses are defined as the base values for each one. The switch-on and switch-off angles are restricted to the intervals (−7°, 9°) and (18°, 28°), respectively. The variation step is chosen as 0.1°.

Fig. 5 shows the optimum switching angles with respect to reference current and motor speed.

5 The proposed controller's block diagram

Once the optimum switching angles are obtained from Eq. (19), they are stored in lookup tables $\theta_{\text{on}}(I_{ref},\ \omega)$ and $\theta_{\text{off}}(I_{ref},\ \omega)$ to build a MATLAB model of the SRM drive system. Each one of the lookup tables has two inputs (I_{ref}, ω) and one output (one for switch-on angle (θ_{on}) and one for switch- off angle (θ_{off})).

The block diagram of the proposed controller is shown in Fig. 6. The speed error is processed through a proportional-integral (PI) speed controller to generate the reference current. Then, the hysteresis current controller and commutation controller are used to making the phase current tracks the reference current inside the angle interval θ_{on} and θ_{off} by providing the gate drive pulses to the power converter.

6 Results and discution

6.1 Simulation results

The Matlab/Simulink has been used to implement the machine model, and the proposed controller for the tested four phases 8/6 SRM. The proposed controller's simulation results were compared with the analytical method presented in [15] to verify its effectiveness and feasibility. In this paper, as each motor has a different inductance profile, the minimum inductance used in the analytical method was fitted as $(\theta)=ae^{(b\theta)}+ce^{(d\theta)}$, where a = 0.01259, b =0.02411, c = 9.552, and d = 0.2512. The start overlapping angle between the rotor pole and stator pole (θ_m) is set to 7.5°.

Fig. 7 shows the simulation results for different reference speed and load torque. The machine initially accelerates under 12 Nm load torque until the reference speed of 1500 rpm is reached. Then, the reference speed is changed to 2750 rpm at 0.5 sec, and the load torque is decreased to 8 Nm at 0.35 sec. As shown in Fig. 7(a), the proposed controller has a better speed response, especially at high-speed operation.

Fig. 7(b) and (c) exemplify the total electromagnetic torque produced by the proposed controller and analytical formula, respectively. Compression of the torque ripple generated by the tow controllers is shown in Fig. 7(d). It may be observed that the proposed approach generates a lower torque ripple during both transient and steady-state responses compared to the analytical method.

The variation of switching angles is depicted in Fig. 8(a) and (b); as shown in the figures, the switching angles are advanced as the motor speed and reference current increase. The average torque and copper loss are shown in Fig. 9(a) and (b), respectively.

The results show that the proposed controller adjusts the switching angles to realize the desired balance between the average torque, torque ripple, and copper losses. However, the proposed controller produces a bit lower starting torque to minimize the torque ripple and

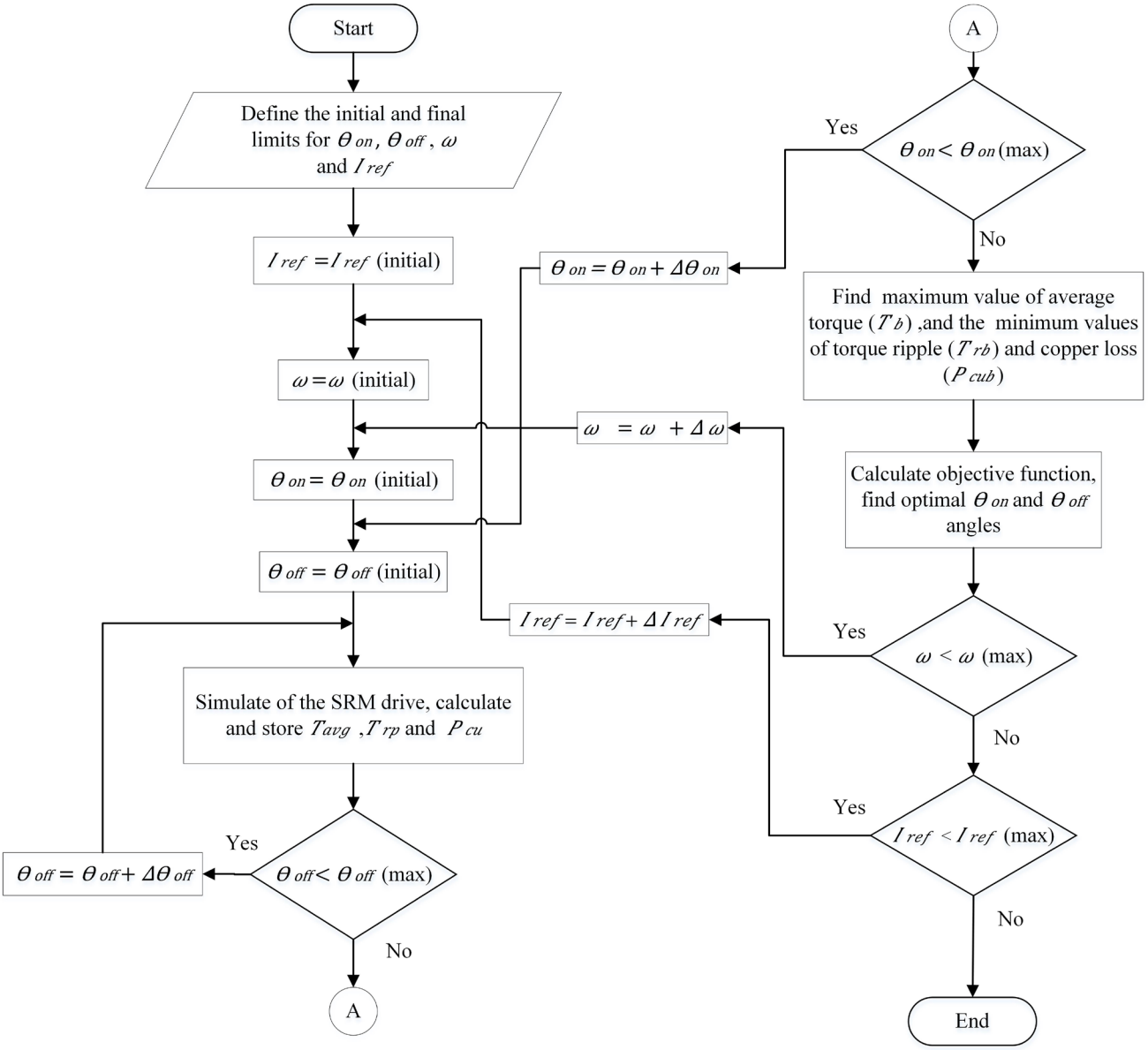

Fig. 4 The flowchart of searching algorithm.

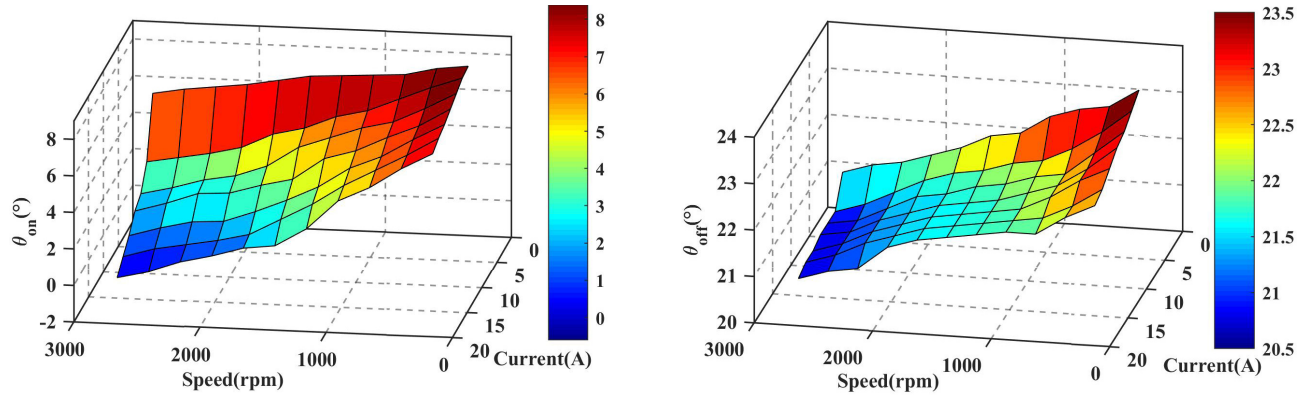

(a) (b)

Fig. 5 Obtained switching angles; (a) switch-on angle; (b) switch-off angle.

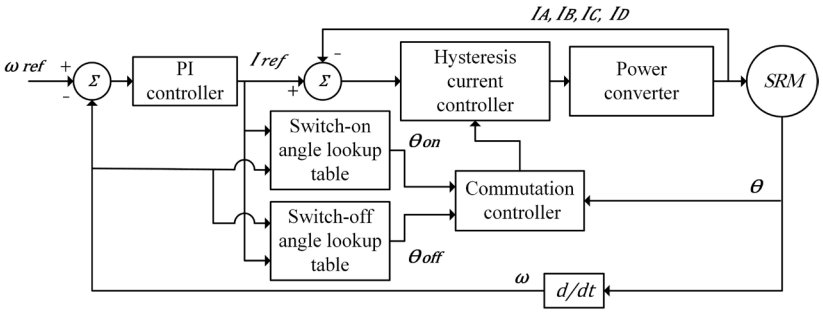

Fig. 6 The block diagram of the proposed controller.

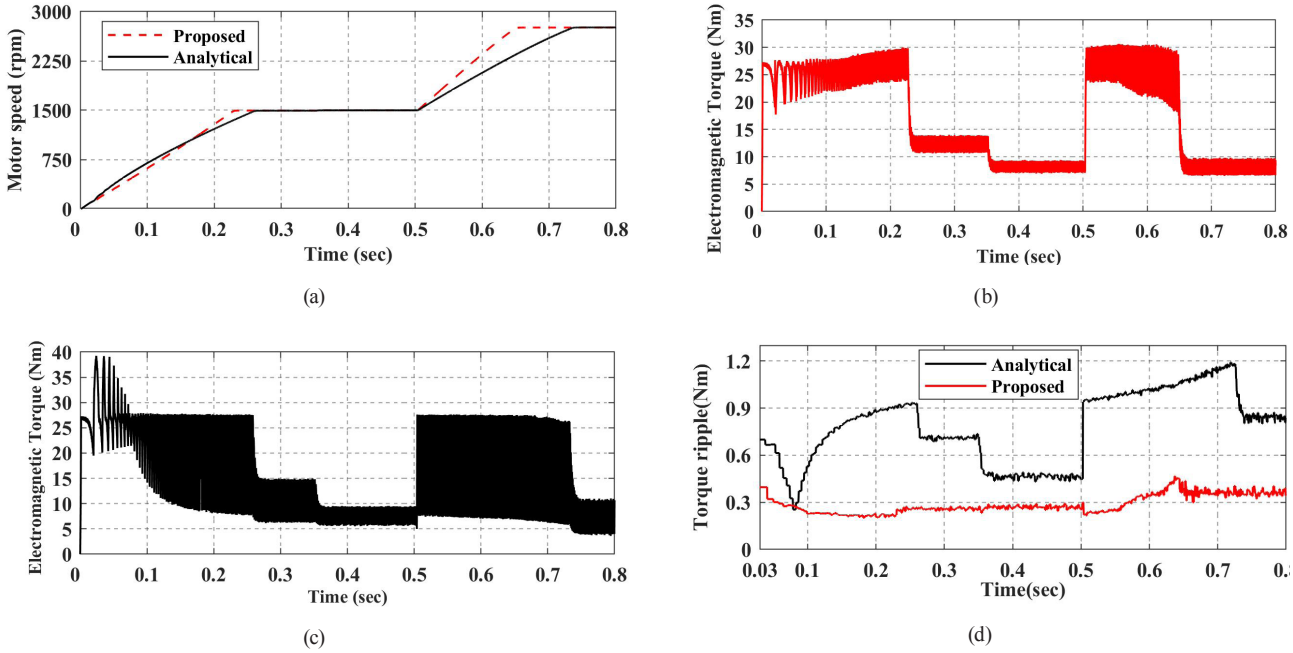

Fig. 7 Simulation results for different reference speed and load torque; (a) Motor speed; (b) Electromagnetic torque for the proposed controller; (c) Electromagnetic torque for the analytical method; (d) Torque ripple generated by analytical and proposed controller.

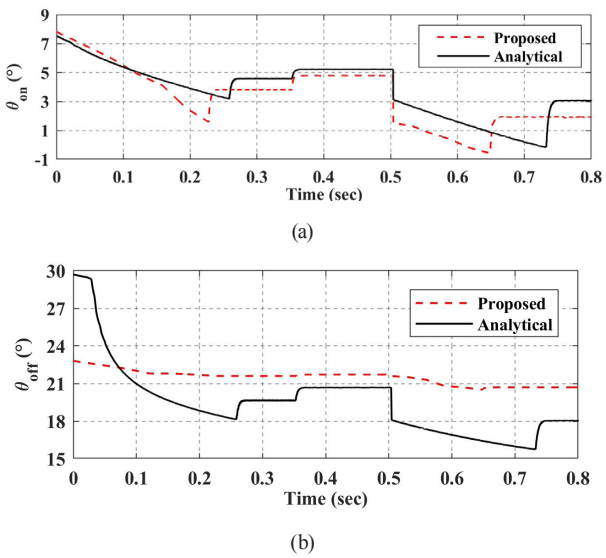

Fig. 8 variation of switching angles; (a) The switch-on angle; (b) The switch-off angle.

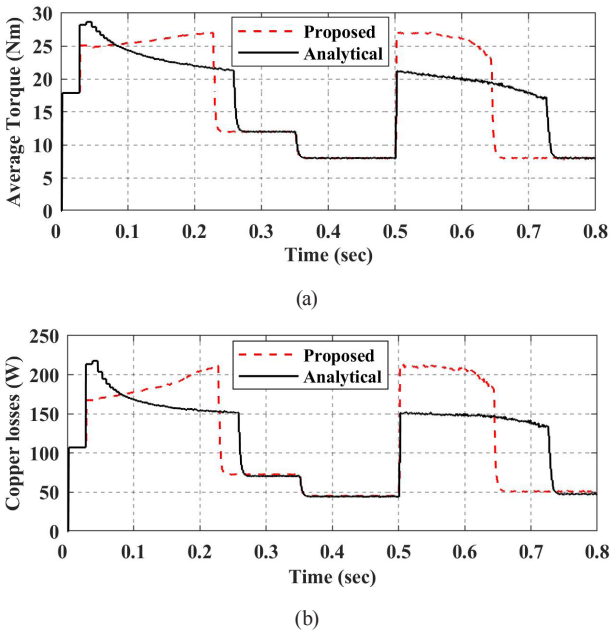

Fig. 9 Simulation results for different reference speed and load torque; (a) The average Torque; (b) The copper loses.

copper losses. After that, the proposed controller produces higher average torque with lower torque ripple and somewhat consumes higher power losses as the weight factor of average torque and torque ripple are greater than copper losses in the objective function.

The phase current and its position for the two controllers are given in Fig. 10. As can be noted, the phase current always reaches its peak at θ_m(7.5°) and decay to zero at θ_z (30°) in the analytical method. In contrast, the positions of peak and decay to zero are varied in the proposed controller with the rotor speed.

6.2 Experimental verification

The proposed and analytical controllers have been experimentally tested to verify the simulation results for the same SRM, as shown in Fig. 11. An electromagnetic brake connected to the SRM serves as a mechanical load. A DSP

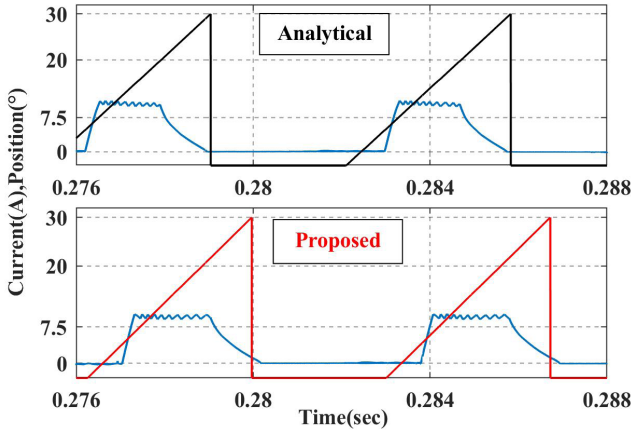

(a)

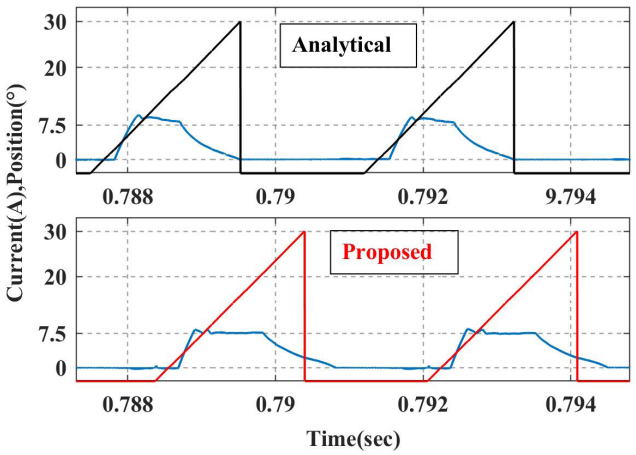

(b)

Fig. 10 Phase current waveform with rotor position; (a) At ω = 1500 rpm; (b) At ω = 2750 rpm.

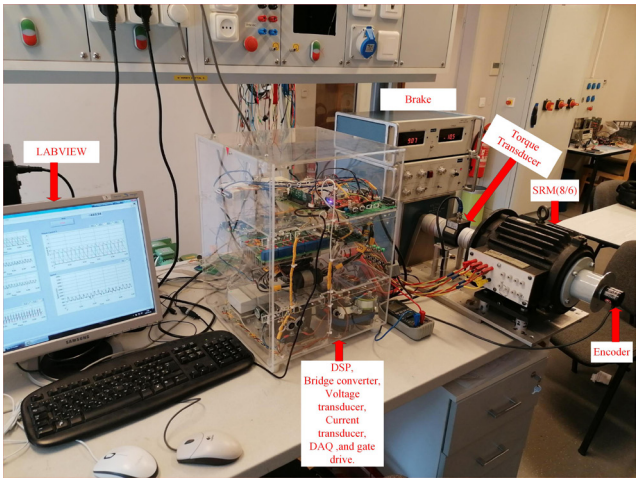

Fig. 11 The measurement platform.

board (TMS320F28335), an asymmetrical bridge converter, an incremental encoder, a current sensor (LAH 50-P), and voltage and torque transducers were set up to obtain the experimental results. The LabView software and data acquisition board (DAQ NI USB-6009) were used to collect and plot the data.

Figs. 12 and 13 show a comparison between the steady state simulation and experiment results for the total electromagnetic torque and phases' current at 700 rpm with 130 v supply voltage.

As is obvious, the proposed controller generates higher torque with a lower torque ripple and almost consumes the same amount of power. Furthermore the experiment results match the simulation results.

7 Conclusions

This paper presents a simple and low-cost control of SRM drive for EV applications based on an optimization algorithm over a wide speed range. The optimum values of switching angles are obtained offline by solving a multi-objective optimization function to realize the maximum average torque and minimum torque ripple, and copper losses. The proposed controller utilizes the obtained values to adjust the switching angle according to the rotor speed and reference current. Comparison of simulation and experiment results between the proposed controller and analytical method show that the proposed controller effectively controls the motor speed under different load values and enhance the drive performance by achieving the desired balance between the average torque, torque ripple, and copper losses.

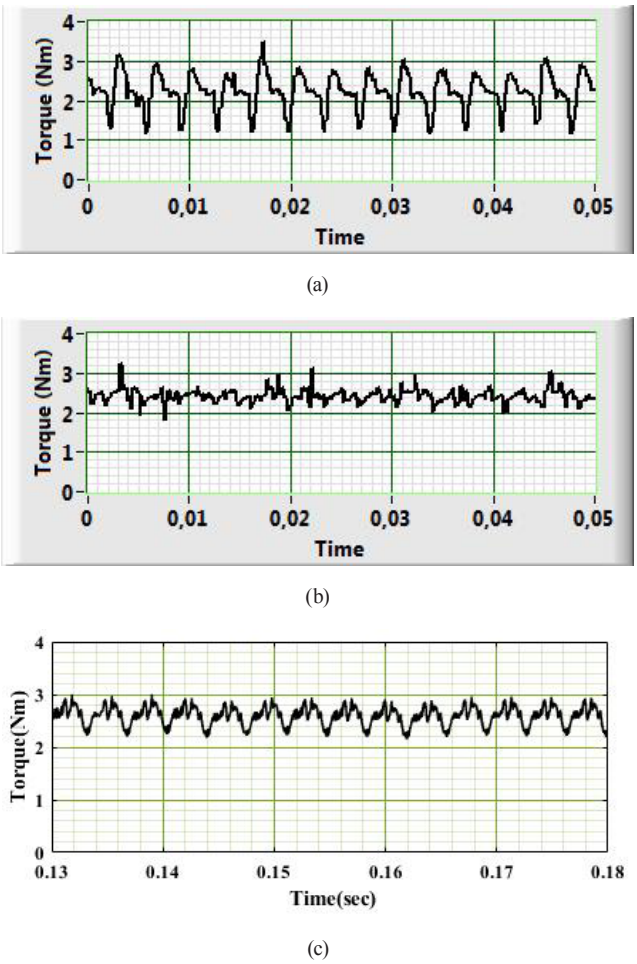

Fig. 12 The simulation and experiment results of the electromagnetic torque; (a) Experimental electromagnetic torque for the Analytical method ($\theta_{on} = 4.3$, $\theta_{off} = 19.5$); (b) Experimental electromagnetic torque for the proposed controller ($\theta_{on} = 7.2$, $\theta_{off} = 23$); (c) Simulated electromagnetic torque for the proposed controller.

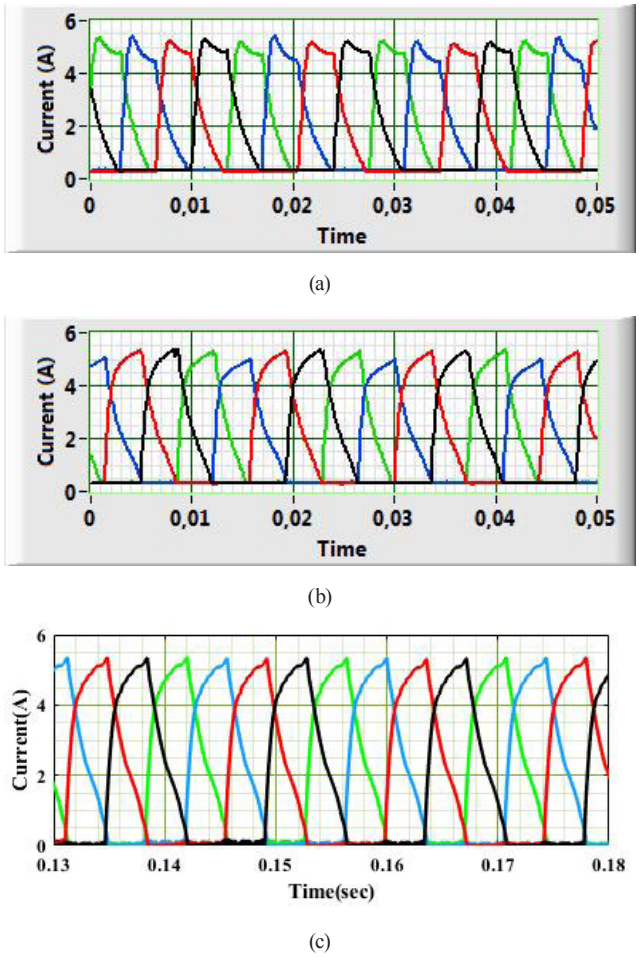

Fig. 13 The simulation and experiment results of the phases' currents; (a) Phases' currents for the Analytical method; (b) Phases' currents for the proposed controller; (c) Simulated phases' currents for the proposed controller.

References

[1] Sun, Q., Wu, J., Gan, C., Si, J., Guo, J., Hu, Y. "Cascaded Multiport Converter for SRM-Based Hybrid Electrical Vehicle Applications", IEEE Transactions on Power Electronics, 34(12), pp. 11940–11951, 2019.
https://doi.org/10.1109/TPEL.2019.2909187

[2] Aiso, K., Akatsu, K. "High speed SRM using vector control for electric vehicle", CES Transactions on Electrical Machines and Systems, 4(1), pp. 61–68, 2020.
https://doi.org/10.30941/cestems.2020.00009

[3] Hu, K. W., Yi, P. H., Liaw, C. M. "An EV SRM Drive Powered by Battery/Supercapacitor With G2V and V2H/V2G Capabilities", IEEE Transactions on Industrial Electronics, 62(8), pp. 4714–4727, 2015.
https://doi.org/10.1109/TIE.2015.2396873

[4] Hamouda, M., Számel, L. Alquraan, L. "Maximum Torque per Ampere based Indirect Instantaneous Torque Control for Switched Reluctance Motor", In: 2019 IEEE 2nd International Conference and Workshop in Óbuda on Electrical and Power Engineering (CANDO-EPE), Budapest, Hungary, 2019, pp. 47–54.
https://doi.org/10.1109/CANDO-EPE47959.2019.9110963

[5] Saha, N., Panda, A. K., Panda, S. "Speed control with torque ripple reduction of switched reluctance motor by many optimizing liaison technique", Journal of Electrical Systems and Information Technology, 5(3), pp. 829–842, 2018.
https://doi.org/10.1016/j.jesit.2016.12.013

[6] Lukman, G. F., Nguyen, X. S., Ahn, J. W. "Design of a Low Torque Ripple Three-Phase SRM for Automotive Shift-by-Wire Actuator", Energies, 13(9), Article number: 2329, 2020.
https://doi.org/10.3390/en13092329

[7] Ye, J., Bilgin, B., Emadi, A. "An Extended-Speed Low-Ripple Torque Control of Switched Reluctance Motor Drives", IEEE Transactions on Power Electronics, 30(3), pp. 1457–1470, 2015. https://doi.org/10.1109/TPEL.2014.2316272

[8] Zhang, W., Xu, A., Han, L., Wang, S. "Minimising torque ripple of SRM by applying DB-DTFC", IET Electric Power Applications, 13(11), pp. 1883–1890, 2019. https://doi.org/10.1049/iet-epa.2018.5441

[9] Divandari, M., Rezaie, B., Ranjbar Noei, A. "Speed control of switched reluctance motor via fuzzy fast terminal sliding-mode control", Computers and Electrical Engineering, 80, Article number: 106472, 2019. https://doi.org/10.1016/j.compeleceng.2019.106472

[10] Kachapornkul, S., Jitkreeyarn, P., Somsiri, P., Tungpimolrut, K., Akira, C., Tadashi, F. "A design of 15 kW switched reluctance motor for electric vehicle applications", In: 2007 International Conference on Electrical Machines and Systems (ICEMS), Seoul, Korea, 2007, pp. 1690–1693. https://doi.org/10.1109/icems12746.2007.4412318

[11] Cheng, H., Chen, H., Yang, Z. "Average torque control of switched reluctance machine drives for electric vehicles", IET Electric Power Applications, 9(7), pp. 459–468, 2015. https://doi.org/10.1049/iet-epa.2014.0424

[12] Sozer, Y., Torrey, D. A., Mese, E. "Automatic control of excitation parameters for switched-reluctance motor drives", In: – Seventeenth Annuel IEEE Applied Power Electronics Conference and Exposition (APEC), Texas, Usa, 2002, pp. 48–56. https://doi.org/10.1109/apec.2002.989226

[13] Hamouda, M., Számel, L. "Optimum Excitation Angles for Switched Reluctance Motor Drives", In: XXXIII. Kandó Conference 2017: "Kandó a tudomány hajóján", Budapest, Hungary, 2017, pp. 128–142.

[14] Hamouda, M., Számel, L. "A new technique for optimum excitation of switched reluctance motor drives over a wide speed range", Turkish Journal of Electrical Engineering & Computer Sciences, 26(5), pp. 2753–2767, 2018. https://doi.org/10.3906/elk-1712-153

[15] Xu, Y. Z., Zhong, R., Chen, L., Lu, S. L. "Analytical method to optimise turn-on angle and turn-off angle for switched reluctance motor drives", IET Electric Power Applications, 6(9), pp. 593–603, 2012. https://doi.org/10.1049/iet-epa.2012.0157

[16] Shahabi, A., Rashidi, A., Afshoon, M., Saghaian Nejad, S. M. "Commutation angles adjustment in SRM drives to reduce torque ripple below the motor base speed", Turkish Journal of Electrical Engineering and Computer Sciences, 24(2), pp. 669–682, 2016. https://doi.org/10.3906/elk-1309-47

[17] Mademlis, C., Kioskeridis, I. "Performance optimization in switched reluctance motor drives with online commutation angle control", IEEE Transactions on Energy Conversion, 18(3), pp. 448–457, 2003. https://doi.org/10.1109/TEC.2003.815854

[18] Jiang, J. W., Peng, F., Bilgin, B., Emadi, A. "Optimisation-based procedure for characterising switched reluctance motors", IET Electric Power Applications, 11(8), pp. 1366–1375, 2017. https://doi.org/10.1049/iet-epa.2017.0072

[19] Labiod, C., Srairi, K., Mahdad, B., Benchouia, M. T., Benbouzid, M. E. H. "Speed Control of 8/6 Switched Reluctance Motor with Torque Ripple Reduction Taking into Account Magnetic Saturation Effects", Energy Procedia, 74, pp. 112–121, 2015. https://doi.org/10.1016/j.egypro.2015.07.530

[20] Xudong, G., Na, R., Chengyu, J., Xudong, W., Yongqin, Z. "Multi-objective optimization of switched reluctance motor drive in electric vehicles", Computers and Electrical Engineering, 70, pp. 914–930, 2018. https://doi.org/10.1016/j.compeleceng.2017.12.016

[21] Yu, C., Xiao, Z., Huang, Y., Zhu, Y. "Two-step commutation control of switched reluctance motor based on PWM", The Journal of Engineering, 2019(22), pp. 8414–8418, 2019. https://doi.org/10.1049/joe.2019.1106

[22] Kioskeridis, I., Mademlis, C. "Maximum efficiency in single-pulse controlled switched reluctance motor drives", IEEE Transactions on Energy Conversion, 20(4), pp. 809–817, 2005. https://doi.org/10.1109/TEC.2005.853738

[23] Correa, D. A. P., Nabeta, S. I., Pereira, F. H., da Silva, J. A., da Silva, W. M. "FEM-coupled simulations and genetic algorithm model applied to reduce the torque ripple of a 2-phase SR motor drive", The Journal of Engineering, 2019(17), pp. 3705–3708, 2019. https://doi.org/10.1049/joe.2018.8007

[24] Likun, H., Qingxin, Y., Jinlong, A. "Modeling of SRM Based on XS-LSSVR Optimized by GDS", IEEE Transactions on Applied Superconductivity, 20(3), pp. 1102–1105, 2010. https://doi.org/10.1109/TASC.2010.2043518

[25] Mihic, D. S., Terzic, M. V., Vukosavic, S. N. "A New Nonlinear Analytical Model of the SRM With Included Multiphase Coupling", IEEE Transactions on Energy Conversion, 32(4), pp. 322–1334, 2017. https://doi.org/10.1109/TEC.2017.2707587

[26] Song, S., Ge, L., Ma, S., Zhang, M., Wang, L. "Accurate Measurement and Detailed Evaluation of Static Electromagnetic Characteristics of Switched Reluctance Machines", IEEE Transactions on Instrumentation and Measurement, 64(3), pp. 704–714, 2015. https://doi.org/10.1109/TIM.2014.2358132

[27] Hamouda, M., Számel, L. "Accurate Magnetic Characterization Based Model Development for Switched Reluctance Machine", Periodica Polytechnica Electrical Engineering and Computer Science, 63(3), pp. 202–212, 2019. https://doi.org/10.3311/PPee.14012

[28] Abdel-Fadil, R. Számel, L. "Predictive Direct Torque Control of Switched Reluctance Motor for Electric Vehicles Drives", Periodica Polytechnica Electrical Engineering and Computer Science, 64(3), pp. 264–273, 2020. https://doi.org/10.3311/PPee.15496

[29] Zhang, P., Cassani, P. A., Williamson, S. S. "An Accurate Inductance Profile Measurement Technique for Switched Reluctance Machines", IEEE Transactions on Industrial Electronics, 57(9), pp. 2972–2979, 2010. https://doi.org/10.1109/TIE.2010.2048831